

# On the Drawing Behavior and Characteristics of Laser Drawn Polypropylene Fibers

Ahmed Jalal Uddin<sup>a</sup>, Yusuke Mashima<sup>a</sup>, Yutaka Ohkoshi<sup>a</sup>, Yasuo Gotoh<sup>a</sup>, Masanobu Nagura<sup>a</sup>,  
Akinobu Sakamoto<sup>b</sup>, Ryuma Kuroda<sup>b</sup>

<sup>a</sup> Faculty of Textile Science & Technology, Shinshu University, Ueda, Nagano 386-8567, Japan

<sup>b</sup> Sumitomo Chemical Co. Ltd., 2-1 Kitasode, Sodegaura, Chiba 299-0295, Japan

## ABSTRACT

Drawing behavior, flow drawing and neck drawing, was studied for i-PP fibers in CO<sub>2</sub> laser drawing system, and the fiber structure and the mechanical properties of drawn fibers were analyzed. For a certain laser power, flow drawing of PP was possible up to draw ratio 19.5. Though the drawing stress was very low, the flow-drawn PP fiber exhibited oriented crystal structure and improved mechanical properties. On the other hand, neck-drawing was accomplished from draw ratio (DR) 4 to 12 with significant increase in drawing stress that enhanced the development of fiber structure and mechanical properties. Unlike PET, the drawing stress depends not only on the draw ratio, but irradiated laser power also. The 10 to 12 times neck drawn fibers were highly fibrillated. The fibers having tensile strength 910 MPa, initial modulus 11 GPa and dynamic modulus 14 GPa were obtained by single-step laser drawing system.

Keywords: Polypropylene fiber, CO<sub>2</sub> laser-heated drawing, flow drawing, neck drawing, fibrillization

## INTRODUCTION

Isotactic polypropylene (iPP) is an outstanding thermoplastic polymer concerning its excellent cost/ performance ratio and high stiffness.<sup>1</sup> Polypropylene (PP) fibers and filaments are used in making a variety of products, such as ropes, cords, nets, woven bags, tents, geotextile components, nonwoven fabrics and reinforcing materials for various composites.<sup>2-3</sup> As a reinforcing component, PP has received an extensive attention because of its lower density than steel fibers and relatively superior strength with respect to other conventional polymers. However, the modulus and tenacity of PP fibers are lower than those of steel fibers by an order of magnitude.<sup>4</sup>

As is commonly known, high modulus and high strength can be achieved by the aligning and straightening of polymer molecules in an axial direction. Based on this, various methods

---

Correspondence to: Y. Ohkoshi  
(E-mail: [yokoshi@shinshu-u.ac.jp](mailto:yokoshi@shinshu-u.ac.jp))

have been adopted till now to enhance the performance of PP fiber such as zone-drawing/zone-annealing,<sup>5</sup> coextrusion method,<sup>6</sup> continuous vibrating zone-drawing<sup>7</sup> etc. In all the methods, at least two or multiple stages of drawing or annealing were required. In this work, we have drawn the PP fibres in a single-step laser-heated drawing system. To obtain a high-strength and high-modulus fiber, the CO<sub>2</sub> laser-heated drawing system has recently been proved to be a very effective technique and is well documented in the literatures for PET and nylon 6.<sup>8-13</sup> But the work of PP dealing with the laser-heated drawing is still sparse.

External heating devices conventionally used for fiber drawing, such as hot roller or hot pin, or a heating region; namely a zone heater, are unable to heat the fiber evenly and instantaneously. Moreover, quick heating to the central part of fiber is hampered and a remarkable temperature difference occurred in the cross-section of the fiber resulting in a disproportionate deformation and inhomogeneous fiber structure. Conversely, if material has a moderate absorption factor, the fiber can be radiantly heated with CO<sub>2</sub> laser drawing system. An instant, uniform and stable neck drawing within a very short range of 0.2 mm can be possible which enhances to obtain a high strength and high modulus fiber. More importantly, CO<sub>2</sub> laser-heated drawing is a single-step of fiber drawing which is very attractive in the economic point of view.

The present work was undertaken to investigate the fiber structure development and the achievement in mechanical properties of PP by utilizing laser-heated drawing. In addition, we examined the flow drawing of PP fiber by laser-drawing system with the objective of preparing microfiber and also to study the elongational behavior of molecular chains in nearly to the molten state. This article starts with a brief discussion on the flow-drawing behavior of PP fiber. The later part discusses the concomitant developments in structure and properties of the subsequently neck drawn fibers in terms of draw ratio.

## EXPERIMENTAL

### Material

PP pellet used in this study, supplied by Sumitomo Kagaku Kogyu Co., Japan, was the commercial grade of W101 having a melt flow rate (MFR) of 10 g/10min,  $\overline{M}_w = 240,000$ ,  $\overline{M}_n = 70,000$  and  $\overline{M}_w / \overline{M}_n = 3.4$ .

### Melt Spinning

PP pellet was extruded at 270° C from a single-hole spinneret having a diameter of 1 mm and an aspect ratio (L/D) of 5. For flow drawing, as-spun fiber of 150 μm diameter was made by adjusting throughput rate of 3.72 g min<sup>-1</sup> at take-up velocity of 250 m min<sup>-1</sup>. As-spun fiber of

diameter around 500  $\mu\text{m}$  was prepared for neck drawing at throughput rate of 5.42  $\text{g min}^{-1}$  and at take-up velocity of 32  $\text{m min}^{-1}$ . The spinning room temperature was 27° C.

### **Laser-Heated Drawing**

Drawing of PP fibers was conducted with a CO<sub>2</sub> laser-heated drawing system. Figure 1a schematically shows the laser drawing system used here. In our previous works<sup>8-9,12-16</sup>, the laser drawing device was used where fiber was run horizontally, laser generator was positioned vertically and laser beam was diffracted from the top to the running fiber. The fiber temperature profiles in the vicinity of neck like deformation was measured and found that for the fiber diameter of 50  $\mu\text{m}$  or more, a shadow of undiffracted laser beam appeared in the rear side of incident ray.<sup>15</sup> In addition, stable flow-drawing was difficult to attain in that horizontal drawing system, because running fiber sagged under its own weight due to no drawing tension imposed on the fiber during flow drawing.<sup>16</sup>

The aforementioned inconveniences were overcome in our newly designed laser drawing device. As shown in Fig 1a, fiber is continuously passed vertically from a feed roller to a wind-up roller at a distance of 1.6 m apart, and the drawing is performed in between these two rollers by irradiating running fiber with a laser beam generator placed horizontally at a distance 0.7 m from the feed roller. In case of drawing of thick fiber, the homogeneous heating was assured by using a multi-directional laser irradiation system as shown in Fig 1b. The fiber is irradiated from surrounding 9-directions by reflecting incident beam from the 16-positioned mirrors in different angles.

During neck drawing<sup>16</sup> of PP, we used multi-directional laser beam system with a view to draw a thick as-spun fiber for obtaining a high draw ratio. For flow-drawing<sup>16-17</sup>, unidirectional laser beam was used. The draw ratio was determined by the following equation:

$$\text{Draw ratio} = (d_0 / d)^2$$

where  $d_0$  and  $d$  are the diameter of as-spun and drawn fibers respectively where the fiber density was assumed to be constant. The employed laser generator was PIN-30S, produced by Onizca Glass Co. Ltd, Japan, having a laser beam of 10.6  $\mu\text{m}$  wavelength, 30 W nominal power, 6.0 mm nominal beam diameter (defined by  $1/e^2$  of maximum intensity), 0.1 mrad nominal beam divergence angle, and random polarization. The laser power was measured by AN/2 laser power meter made of Ophir Co. Ltd., Japan. A lens with 127 mm focal length was used to converge the laser beam and the beam diameter was set up by changing the distance between the lens and the fiber. During neck drawing of PP, lens was removed from the beam line and direct beam was used for multidirectional reflection. During flow drawing, the laser beam diameter at the drawing point was set up at 4 mm. The beam power was respectively 10~16 W and 30 W for flow drawing and neck drawing.

In both the cases of flow drawing and neck drawing, a tension meter, as shown in Figure 1a, was incorporated in the drawing line for measurement of on-line drawing tension. Drawing stress was ascertained by dividing drawing tension with the cross-sectional area of drawn fiber.

## Measurements

**Drawing Tension:** The tension meter used for measuring drawing tension for every 100 ms during flow drawing was a Toray Engineering TTM-201 type tension meter equipped with a 100-gf pick-up. In case of neck drawing, the tension meter was an EIKO SOKKI model 1500 which can pick-up the tension up to 1 kgf.

**Birefringence:** Birefringence was obtained by measuring the refractive indices parallel and perpendicular to the fiber axis by an Interphako Interference Microscope, Carl Zeiss JENA Ltd., Germany. During each measurement, five fibers were randomly taken from different positions and then averaged.

**Wide-angle X-ray Photographs:** Wide-angle X-ray diffraction (WAXD) photographs were taken with a Rigaku Geigerflex 2028 X-ray generator operated at 40 kV and 20 mA. The radiation was Ni-filtered Cu-K $_{\alpha}$  (wavelength 1.542 Å).

**Wide-angle X-ray Profiles, Crystal and Amorphous Orientation:** The equatorial WAXD profiles of as-spun and drawn samples were taken and the changes in crystal orientation ( $f_c$ ) with laser-drawing were determined from the intense peak corresponding to (110) plane. Curves derived from the azimuthal scans were fitted to the profiles of mathematical model investigated using Gauss functions<sup>18</sup> as mentioned in equation (1), where  $I_o$  is peak intensity,  $\phi_o$  is the azimuthal angle at  $I_o$  and  $\tau$  is the peak width. Crystal orientation function was then obtained according to the equation (2).

$$I_{(\phi)} = I_o \exp \left\{ - \left( \frac{\phi - \phi_o}{\tau} \right)^2 \right\} \quad (1)$$

$$f_c = \frac{3 \langle \cos^2 \phi \rangle - 1}{2} \quad (2)$$

$$\text{where} \quad \langle \cos^2 \phi \rangle = \frac{\int_0^{\pi/2} I_{(\phi)} \cos^2 \phi \sin \phi d\phi}{\int_0^{\pi/2} I_{(\phi)} \sin \phi d\phi}$$

Ni-filtered Cu-K $\alpha$  X-ray source, produced by a Rigaku Rota flex 200B and operated at 40 kV and 150 mA, was used during these observations.

**Density:** Using a mixture of methanol and water, the fiber density was measured by the floatation method. Each density value represents the average of three measurements. Volume fraction crystallinity was calculated from density values, using the following equation

$$X_v = (\rho - \rho_a) / (\rho_c - \rho_a)$$

where  $\rho$ ,  $\rho_c$ , and  $\rho_a$  are the densities of the fibers, the crystalline phase, and the amorphous phase, respectively. The values of 0.936 and 0.853 g cm $^{-3}$  were used here for  $\rho_c$  and  $\rho_a$  values.<sup>19</sup>

**Scanning Electron Micrograph:** To analyze the morphological changes of fibrillated sample, fractured PP fibers were collected after tensile testing. Specimens were coated with a Pd-Au sputtering. The fractured fiber surfaces were then observed with a HITACHI S-2460 scanning electron microscope (SEM).

**Mechanical Properties:** Tensile properties of filament fibers (50 mm gauge length) were measured in Tensilon Model RTC-1250A, Japan at a crosshead speed of 50 mm min $^{-1}$ . The experimental results represent the average of 10 individual measurements.

**Dynamic Mechanical Properties:** The dynamic viscoelastic properties were measured by an ITK Co. DVA-225 instrument at a frequency of 10 Hz and a heating rate of 10°C min $^{-1}$  on fibers of 20 mm length. The lower temperature relaxations were performed in a stream of dry air cooled by liquid nitrogen at atmospheric pressure.

## RESULTS AND DISCUSSION

### Drawing Stress

The drawing stress of PP fiber as a function of laser power and draw ratio was first observed. The multi-directional laser irradiation system was used with 500  $\mu$ m as-spun fiber. For a particular draw ratio, laser power was gradually raised and the respective drawing stress was recorded which is shown in Fig. 2. It was found that the drawing stress decreased with the increase in laser power though the draw ratio was fixed. This type of phenomenon was not observed for laser-drawn PET fiber.

At high laser power, in between neck drawing and melting, the molecular system of linear chain PP seemed to be very flexible and its molecular movement might be comparatively easier that resulted the decrease in drawing stress. We tried for flow drawing of PP in that particular condition.

### Flow Drawing of PP Fiber

Figure 3 shows the profiles of the flow drawing of PP as a function of draw ratio and drawing tension. The drawing was initiated from neck state at draw ratio 3, drawing feed speed  $2 \text{ m min}^{-1}$  and laser power (LP) 10 W. Laser power and drawing take-up velocity were simultaneously increased very slowly, LP was fixed in a certain point, such as 11 W, 12 W and so on. At the same time, the draw ratio was increased by increasing take-up velocity along with observation of drawing point whether neck point transforms into flow state. After transformation of neck point into flow, drawing stress suddenly dropped and the draw ratio was increased in that state by increasing take-up velocity. Flow drawing could not be possible in case of laser power 10 to 14 W and 16 W, rather fiber breaking was observed due to high drawing stress. The flow drawing was only possible at laser power 15W and four datas of 15 W are illustrated in Figure 3. The highest possible draw ratio was achieved at 19.5 times and at draw ratio of 19.5 (sample 4 in Fig. 3), drawing stress again started to increase and fiber broke immediately after re-appearance of neck point.

The flow drawing behavior of PP is alike with the same of PET in the sense that the drawing state transforms between flow drawing and neck drawing catastrophically.<sup>16</sup> In accordance to our previous work,<sup>17</sup> the approximate fiber temperature just next to the laser irradiated point was assumed to be 180-220°C that might exceed the melting temperature of PP, whereas the fiber temperature in the flow-drawing state of PET did not need to increase higher than its melting temperature.<sup>17</sup> The reason behind is that the other common fibres such as PET, Nylon etc. can be flow-drawn above flowing temperature, such as about 115°C for PET, since their as-spun fibres are almost in amorphous form. Unlike those fibres, as-spun PP is crystallized in room temperature and hence it needs a temperature adjacent to melting point to draw the fiber in nearly molten state. For this reason, the term ‘melt drawing’ may be homologous of the term ‘flow drawing’ in case of PP.

Another point regarding flow drawing of PP is that there is no absolute difference found between flow and neck drawing of PP. In case of PET, the as-spun fiber is almost amorphous, and above the flowing temperature, all the molecular chains become very flexible and slip aside very easily during drawing. Hence the PET can be flow-drawn more than hundred times without any remarkable improvement of molecular orientation and crystallinity.<sup>16</sup> Conversely, the PP fiber drawn in molten state crystallizes in its cooling process accompanying with molecular orientation. Hence somewhat developed crystalline structure of as-spun PP fibre might turn to more oriented crystalline structure after flow drawing (Figure 4).

In Fig 4, the WAXD photo of as-spun PP indicates some developed crystalline structure and oriented crystals especially at the (040) and (130) planes. In respect to as-spun fiber, X-ray diffraction arcs in flow drawn sample become more distinct and stronger which reveal some improvement in crystal orientation. The meridional arcs in the same circle of (110) plane

indicates the existence of  $\beta$  or pseudohexagonal crystal forms. However, the molecular chains of PP are linear and its glass transition temperature ( $T_g$ ) is very low, hence the as-spun fiber tends to crystallize at room temperature. As the as-spun PP fiber is crystallized, so it needs the temperature near melting to obtain flow drawing. In our observation, the initial transformation of neck to flow state can be explained as a rubbery deformation of molecules into viscoelastic flow where some small crystals might be flexible or melts and hence the flow drawing was possible. The further re-appearance of neck during breaking can be assumed as a recrystallization of molecules or strain hardening of molecules by saturation of crystal orientation.

In table 1, birefringence and tensile properties of as-spun and flow drawn PP samples are listed. In good agreement with the WAXD photo, birefringence, tensile strength, Young's modulus and elongation of flow drawn sample show quite improved values than those of as-spun fiber. The WAXD pattern and characteristics of flow-drawn PET fiber expressed almost the same of as-spun amorphous fiber.<sup>13</sup> The as-spun of PET was amorphous and so it is possible to flow draw just above  $T_g$ . The resultant flow drawn fiber also remained amorphous because of its higher  $T_g$  than room temperature.

Suzuki et al.<sup>20</sup> also observed oriented crystallites and a high degree of molecular orientation in their produced PP microfiber in molten state. They attributed this fact to the instantaneous plastic flow occurring from molten state that caused strain-induced-crystallization and molecular orientation. The characteristics of flow drawn PP sample are in contrast with the same of PET where the flow-drawn PET fiber showed almost the same structure and properties of amorphous (as-spun) fiber.<sup>13</sup>

## **Neck-Drawn PP fiber**

### **Structure Development**

To analyze the structural development of neck drawn PP fiber during laser drawing, the as-spun fiber was drawn at drawing feed speed  $4 \text{ m min}^{-1}$  at which the highest draw ratio (DR) up to 12 was attained. The drawn fibers at DR 4, 6, 8, 10 and 12 were prepared. Interestingly DR 10 and DR 12 fibers had a noticeable difference in the appearance. The fibers became opaque and appeared to be delustrated. This 'whitening' phenomenon was also earlier observed during two-stage PP drawing at draw ratios more than 7. The reason was investigated and ascribed to the formation of microvoids or longitudinal cavities during drawings.<sup>21,22</sup>

Table 2 lists the different structure parameters of neck-drawn PP fibers including drawing stress. As seen, the drawing stress shows a significant increase with draw ratio. Birefringence increases with draw ratio and for DR 10 and DR 12 white fibers, birefringence could not be measured in optical microscope due to their opacity. Density is found to have increased up to DR 8 and then again decreased for DR 10 and 12. The low density of white fibers is assumed to

be due to intermolecular and interfibrillar free volume or voids. The density values measured by floatation method for DR 10 and DR 12 fibres may be less reliable, hence these values are not listed in Table 2. However, the equivalent volume crystallinity for DR 8 is around 54%. The SEM images, described later as shown in Fig. 7, of white fibers provides evidence of fibrillization. Assuming no existence of void in DR 8 fiber, the void fraction of DR 10 and DR 12 was estimated around 2-3% by  $(1 - \text{density of DR 10 or DR 12 fiber} / \text{density of DR 8 fiber})$ . The crystal orientation factor ( $f_c$ ) measured in (110) plane shows high values and gradual increase with draw ratio especially for DR 6 to DR 12 fibers.

Fig. 5 shows the WAXD photographs of as-spun and neck drawn fibers. As-spun fiber displays isotropic and randomly oriented crystals. By the drawing of 4 times, the crystal orientation was clearly increased and crystal form was assumed to be pseudo-hexagonal ( $\beta$ -form) as found for flow-drawn fiber. At a draw ratio of 6 and above, the diffraction arcs turned into spots and have been very prominent implying that crystallinity and crystal orientation are very highly developed from draw ratio 6. And the crystal form also transformed into monoclinic. The patterns of fibrillated samples of DR 10 and DR 12 represent sharpest spots among all indicating a very well-oriented crystalline structure. Glancing back to the Table 2, it is seen that the crystal orientation factor and drawing stress of these fibrillated samples are highest. The crystallization at high orientation proceeds at a rate many times faster than that at low orientation is promoted in the drawing direction.<sup>23,24</sup> In this connection, the volume crystallinity of DR 10 and DR 12 samples (not listed in Table 1) must be higher than 54% of DR 8 sample.

Equatorial WAXD profiles of drawn samples, shown in Fig. 6, exhibit three strong reflections [(110), (040), and (130)] and two weak reflections [(060) and (220)]. Both the  $\alpha_1$  and  $\alpha_2$  crystal forms have their identical X-ray spectra, and our drawn fibers show  $(h + k)$  an even number expressing the existence of only  $\alpha_1$  crystal form since  $(h + k)$  odd may be present in the  $\alpha_2$  form.<sup>25</sup> No reflections resulting from the  $\beta$ -form [(300) at  $2\theta = 16.10^\circ$ ] and  $\gamma$  form [(113) at  $2\theta = 14.98^\circ$  and (117) at  $20.06^\circ$ ] were observed.<sup>26</sup> WAXD profile of draw ratio 4 sample did not exhibit  $\beta$ -crystal form though its WAXD pattern indicated some sort of  $\beta$ -reflection at meridian. It should be noted here that during our experimentation the WAXD patterns of all drawn samples were taken just after completion of drawing and WAXD profiles were taken some days later. Hence the structure of DR 4 fiber can be assumed as follows. The  $\beta$ -crystal form of PP is very unstable and at draw ratio 4, this may be considered as the transition of crystal form  $\beta$  to  $\alpha$  and co-existence of both crystal form. However, in Fig. 6, the gradual closeness of all peaks with increasing draw ratio may indicate that crystallites in equatorial direction becomes smaller with increasing draw ratio. The conversion of spherulite lamellar structure into an extended microfibrillar form by the high drawing stress can be speculated here.

The SEM image of white fiber, shown in Fig. 7, provides clear information about the occurrences of fibrillization in highly drawn fibers. However, this fibrillated PP fibers are useful

in enhancing the mechanical properties of concrete materials, sound insulator, absorbents, leather substitutes, hygienic materials, curtains, wiping cloths and filters.<sup>27,28</sup>

As detailed above, the structure of neck-drawn fibers are found to develop according to draw ratio which can be attributed to their corresponding drawing stress, shown in Table 1. Improvements in molecular orientation and crystallinity under high spinning stress were reported earlier for the high-speed nylon 6<sup>29</sup> and PET<sup>30</sup> spun fibers.

### **Correlation of Mechanical Properties with Fiber Structure**

Fig. 8 shows the typical stress-strain curves for neck drawn PP fibers as a function of draw ratio. For DR 4 and DR 6 samples, the shape of the stress-strain curves expresses an initial linear portion, a marked yield point and a region of low slope up to the rupture where large extensions are produced by small increase in stress. The DR 8, DR 10 and DR 12 samples exhibit brittle mode of deformation behavior with a short initial period of steep slope, no apparent yield point, and a regime of sharply rising stress until fracturing. A steeper initial slope of these fibers indicate the toughness in their nature i.e., larger initial resistance to the applied stress.

Several tensile properties such as tensile strength, Young's modulus and elongation at break evaluated from the stress-strain curves are summarized in Table 3. In a close agreement with the structure development, tensile properties also show the same improvement with draw ratio. The tensile strength and Young's modulus increase significantly with draw ratio. The breaking elongation of as-spun fiber of 1769% drastically drops to 144 for DR 4 fiber. Increases in further orientation and crystallinity for DR 12 fiber, the breaking elongation decreases noticeably to 15%. A maximum value of 910 MPa was attained for tensile strength which is far higher than that of commercially available fibers, 392-470 MPa.<sup>5</sup> On the other hand, the maximum value of Young's modulus, 11 GPa is almost twice that of the commercial fiber, 5.2-6.0 GPa.<sup>5</sup>

The temperature dependence in mechanical property is brought out by the dynamic viscoelastic analysis. In Fig. 9a the storage modulus ( $E'$ ) and loss tangent ( $\tan \delta$ ) are shown for the temperature range between -150 to +180° C. The  $E'$  values are increased with draw ratio over the whole temperature range and for DR 12 fiber, the maximum value at room temperature (20° C) reaches to approx. 14 GPa. In addition, the fibers of DR 6 to DR 12 exhibit high  $E'$  values even at high temperature: for example, around 5 GPa at 100° C for DR 12 fiber. The increase in  $E'$  with draw ratio may suggest that high levels of molecular orientation and crystallinity achieved with drawing.

Figure 9b shows the temperature dependence of  $\tan \delta$  curves of as-spun and drawn PP fibers. In the lower temperature range, we could not observe any isolated dispersion peak. In the higher temperature range, two dispersion peaks appeared for as-spun and DR 4 fibers. The lower temperature peaks appeared at around 10°C corresponds to the  $\alpha_a$  i.e., amorphous relaxation or glass transition, whereas the higher temperature peak shoulder appeared at 55°C for as-spun

fibre and peak at around 100°C for DR 4 fibre represent the  $\alpha_c$  or crystalline transition.<sup>5</sup> From the molecular viewpoint, the  $\alpha_c$  relaxation can be identified as the c-shear relaxation process, i.e., a c-slip process.<sup>7</sup> The peaks' height of DR 4 sample in compare to the same of as-spun and other higher draw ratio fibre are inexplicable. For the sample drawn at high draw ratio such as DR 8, DR 10 and DR 12, the  $\alpha_a$  peak was completely disappeared and  $\alpha_c$  peak decreases markedly in height and shifts to higher temperatures in accordance with draw ratio. Such behavior may be attributed to the sufficient fibre structure development with the increase in draw ratio.

Wills et al.<sup>31</sup> studied dynamic mechanical behavior of ultra high modulus material obtained for  $\overline{M}_w$  in the range of 180,000 and 400,000 and showed that the drawn sample with high intercrystalline orientation has no  $\alpha_a$  peak (they termed it as  $\beta$ -relaxation). In our study, the absence of  $\alpha_a$  relaxation and the shape and gradual shifting of  $\alpha_c$  peak to higher temperature for the highly drawn samples can be attributed to the development of crystalline structure and orientation of the intercrystalline materials. The highest drawn DR 12 fiber shows the maximum  $\alpha_c$  at 112° C.

## CONCLUSIONS

Some conclusive remarks may be made from the present investigation of the drawing behavior and characterization of PP fibers.

Polypropylene fiber was continuously flow-drawn to a maximum draw ratio of 19.5 with heating by laser irradiation. Despite almost no drawing stress imposed on the draw-line, flow-drawn PP fiber was shown some developed crystalline structure and oriented crystals along with quite an improvement in mechanical properties.

During neck drawing, PP fiber was possible to draw up to 12 times. A significant increase in drawing stress was marked with increasing draw ratio which is believed to enhance the fiber structure and mechanical properties. Pseudohexagonal crystal form of draw ratio 4 turned into monoclinic for draw ratio 6 and over. The 'white' fibers of DR 10 and DR 12 evidently showed fibrillated structure which can be ascribed to the fact of the existence of intermolecular and interfibrillar microvoids. The DR 12 sample showed maximum developed structure and improved mechanical properties in spite of having microvoids. A maximum value of 910 MPa was attained for the tensile strength, 11 for initial modulus and 14 for storage modulus.

The laser-heated drawing used in this study for neck drawing has a multi-directional laser irradiation system to heat the running fiber from the surrounding 9-directions. This type of drawing system can be considered as an ideal fiber drawing system in the light of homogeneous heat distribution of the fiber that enables very stable drawing and subsequently leads the fiber in achieving maximum orientation and orientation-induced crystallization. The monoclinic crystal

structure and mechanical properties of PP fiber in this work can be thought to be good attainment in fiber structure and properties in a single-step laser drawing process.

### **Acknowledgements**

The authority of Sumitomo Chemical Co. Ltd., Japan is gratefully acknowledged for the generous supply of PP pellets. The authors also acknowledge the support of a Grant-in-Aid from the Center of Excellence for 21st Century Research program of the Ministry of Education, Culture, Science and Technology of Japan.

### **REFERENCES AND NOTES**

1. Denac, M.; Musil, V.; Smit, I. *J Polym Sci Part B*, 2004, 42, 1255-1264.
2. Balaguru, P.; Shah, S. P. *Fiber Reinforced Cement Composites*; McGraw-Hill:New York, 1992.
3. Dutra, R. C. L.; Soares, B. G.; Campos, E. A.; De Melo, J. D. G.; Silvia, J. L. G. *J Appl Polym Sci* 1999, 73, 69-73.
4. Lim, J. Y.; Kim, S. Y. *J Polym Sci Part B*, 2003, 41, 1175-1182.
5. Kunugi, T.; Ito, T.; Hashimoto, M.; Ooishi, M. *J Appl Polym Sci* 1983, 28, 179-189.
6. Kunugi, T.; Yoneyama, Y. *J Appl Polym Sci* 1990, 41, 455-465.
7. Suzuki, A.; Sugimura, T.; Kunugi, T. *J Appl Polym Sci* 2001, 81, 600-608.
8. Ikaga, T.; Kobayashi, A.; Ohkoshi, Y.; Gotoh, Y.; Nagura, M.; Urakawa, H.; Kajiwara, K. *Sen'i Gakkaishi* 2002, 58, 8-15.
9. Ikaga, T.; Kobayashi, A.; Ohkoshi, Y.; Gotoh, Y.; Nagura, M. *Sen'i Gakkaishi* 2002, 58, 16-21.
10. Suzuki, A.; Mochiduki, M. *J Appl Polym Sci* 2001, 82, 2775-2783.
11. Suzuki, A.; Ishihara, M. *J Appl Polym Sci* 2002, 83, 1711-1716.
12. Ikaga, T.; Ohkoshi, Y.; Gotoh, Y.; Nagura, M.; Kawahara, Y. *Sen'i Gakkaishi* 2003, 59, 235-238.
13. Okumura, W.; Ohkoshi, Y.; Gotoh, Y.; Nagura, M.; Urakawa, H.; Kajiwara, K. *J Polym Sci Part B*, 2004, 42, 79-90.
14. Uddin, A. J. ; Ohkoshi, Y.; Gotoh, Y.; Nagura, M.; Endo, R.; Hara, T. *J Polym Sci Part B*, 2004, 42, 433-444.
15. Okumura, W.; Yamaguchi, T.; Ohkoshi, Y.; Gotoh, Y.; Nagura, M. *Int Polym Process* 2002, 17, 124-132.
16. Ohkoshi, Y.; Watanabe, J.; Gotoh, Y.; Nagura, M. *Sen'i Gakkaishi* 2002, 58, 182-184.

17. Nam, S.; Watanabe, J.; Okumura, W.; Ohkoshi, Y.; Gotoh, Y.; Nagura, M. Symposium papers of the Japan Society of Polymer Processing, Kanazawa, Japan, Nov 3-2, 2003, pp 381-382.
18. Heuvel, H. M.; Huisman, R.; Lind, K. C. J. B. *J Polym Sci Part B*, 1976, 14, 921-940.
19. Natta, G. *J Polym Sci* 1955, 16, 143-154.
20. Suzuki, A.; Narusue, S. *J Appl Polym Sci* 2004, 92, 1534-1539.
21. Sfiligoj, S. M.; Diana, G. S. *Acta Chimica Slovenica* 2002, 49, 773-782.
22. Maaty, M. I. A. E.; Bassette, D. C.; Olley, R. H.; Dobb, M. G.; Tomka, J. G.; Wang, I. C. *Polymer* 1996, 37, 213-218.
23. Murthy, N. S.; Bray, R. G.; Correals, S. T.; Moore, R. A. F. *Polymer* 1995, 36, 3863-3873.
24. Peszkin, P. N.; Schultz, J. M.; Lin, J. S. *J Polym Sci Part B* 1986, 24, 2592-
25. Kalay, G.; Zhong, Z.; Allan, P.; Bevis, M. J. *Polymer* 1996, 37, 2077-2085.
26. Jacoby, P.; Bersted, B. H.; Kissel, W. J.; Smith, C. E. *J Polym Sci Part B* 1986, 24, 461-
27. Fumio, M.; Shigemitsu, M.; Hiroshi, N. *Jpn. Kokai Tokkyo Koho* 1994, JP 06257011.
28. Parviz, S.; Ataulah, K.; Wen, H. J. *ACI Mater J* 1992, 89, 534-540.
29. Murase, S.; Kashima, K.; Kudo, K.; Hiram, M.; *Macromol. Chem. Phys.*, 1997, 198, 561-572.
30. Hamana, I.; Matsui, M.; Kato, S. *Melliand Textilber*, 1969, 4, 382 and 1969, 5, 499.
31. Wills, A. J.; Capaccio, G.; Ward, I. M. *J Polym Sci Part B* 1980, 18, 493-509.

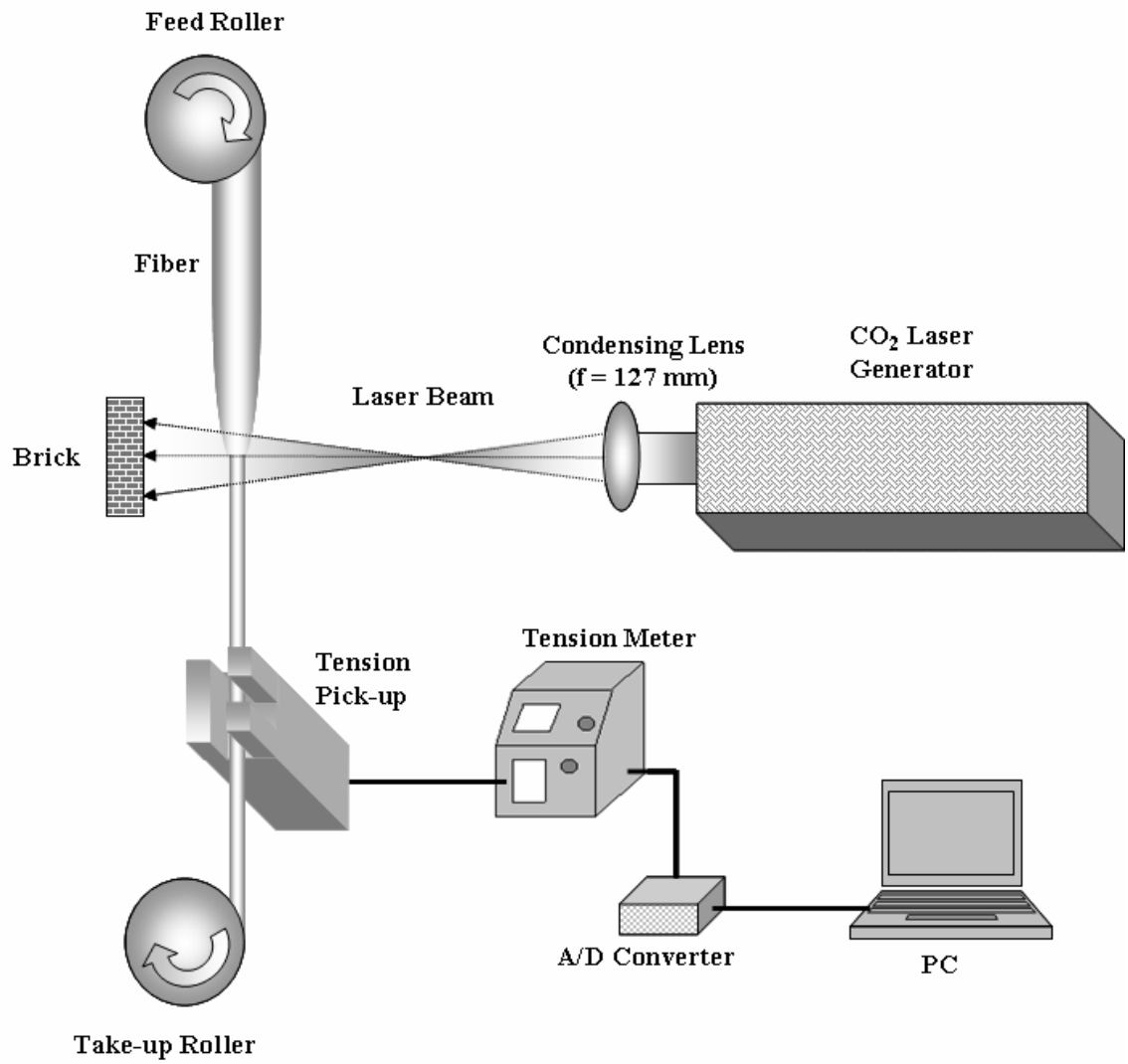


Figure 1a. Schematic diagram of the CO<sub>2</sub> laser-heated-drawing system.

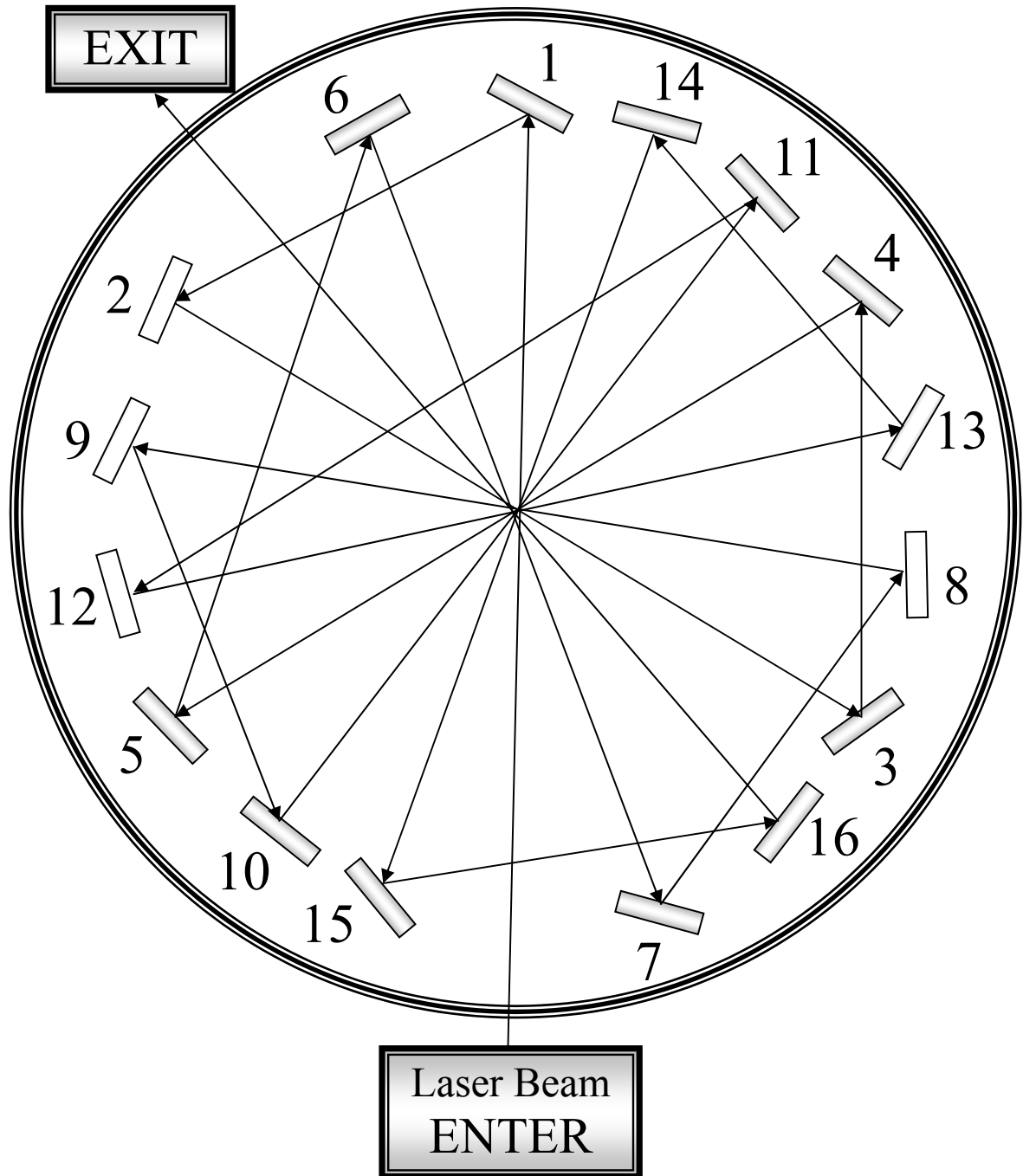


Figure 1b. Schematic diagram (top view) of the multi-directional laser irradiation system. Number 1 to 16 represents corresponding mirror where laser beam is reflected successively. Fiber is run vertically through the centre point of each reflection.

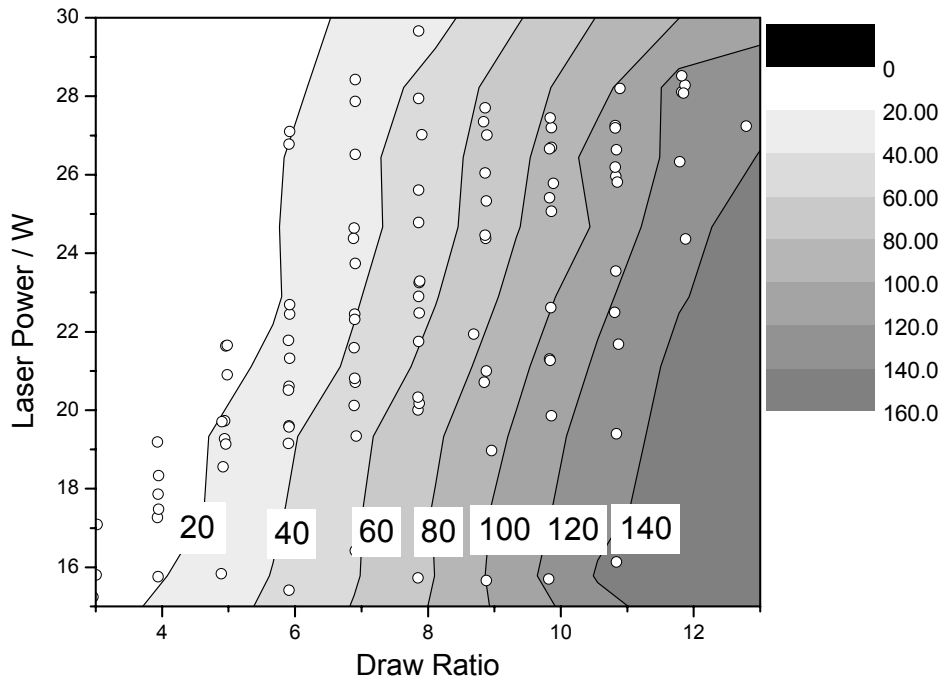


Figure 2. Drawing stress of PP as a function of laser power and draw ratio. Numeral 20 to 140 in the figure indicates drawing stress in MPa.

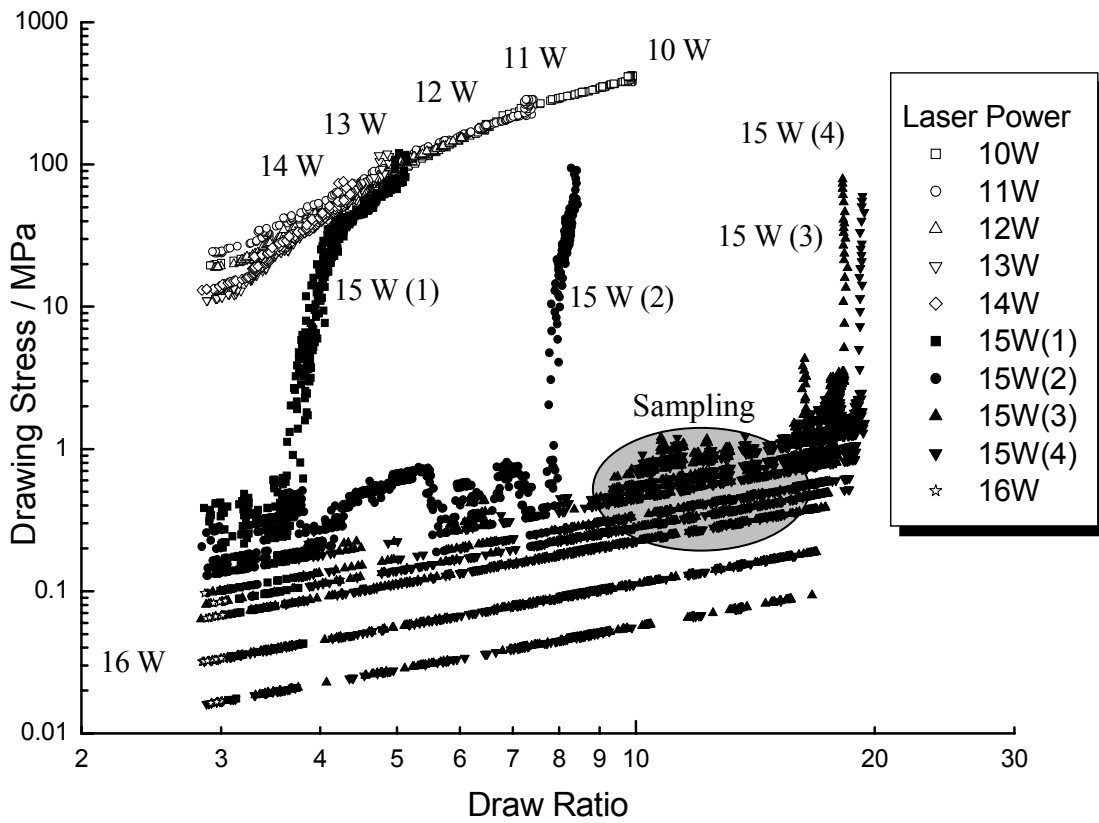


Figure 3. Neck drawing and flow drawing of PP. The drawing stress as a function of laser power and draw ratio is shown.

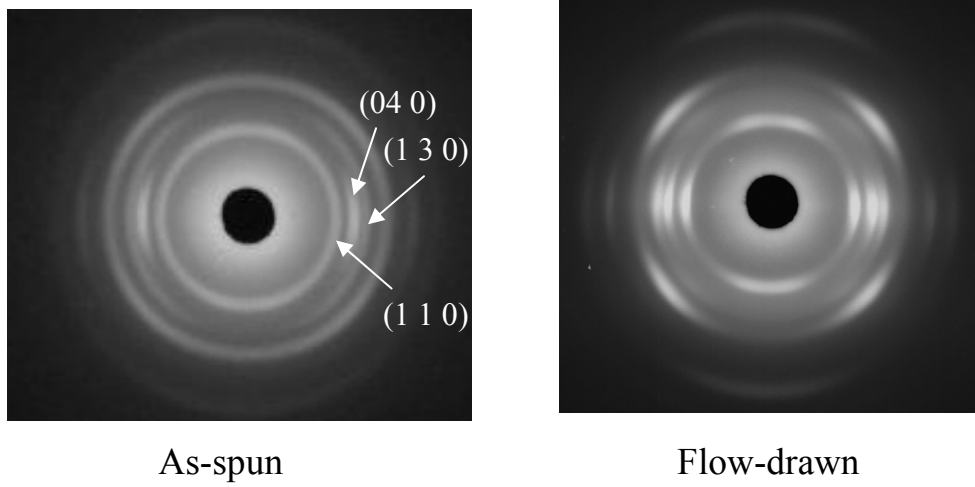


Figure 4. WAXD photographs of as-spun and flow drawn PP fiber.

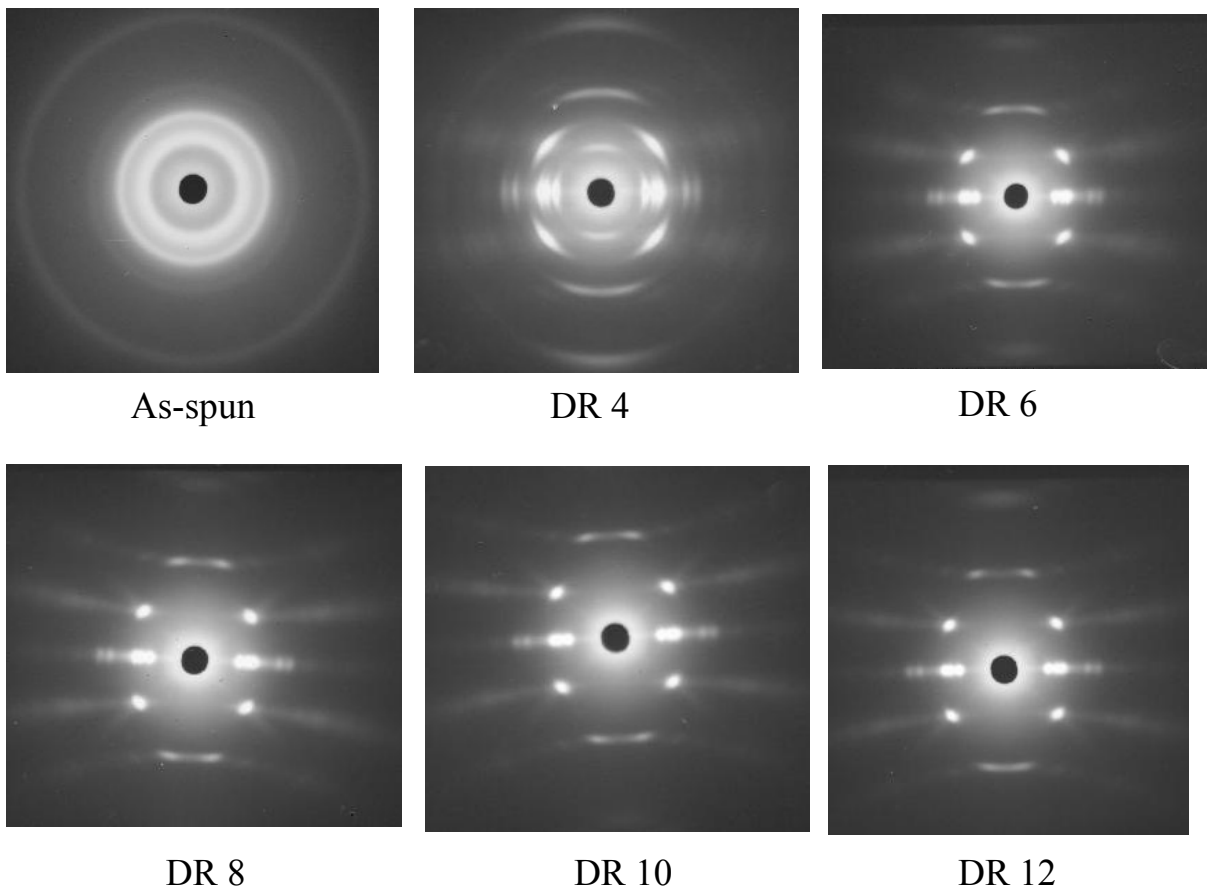


Figure 5. WAXD photographs of as-spun and neck drawn PP fiber.

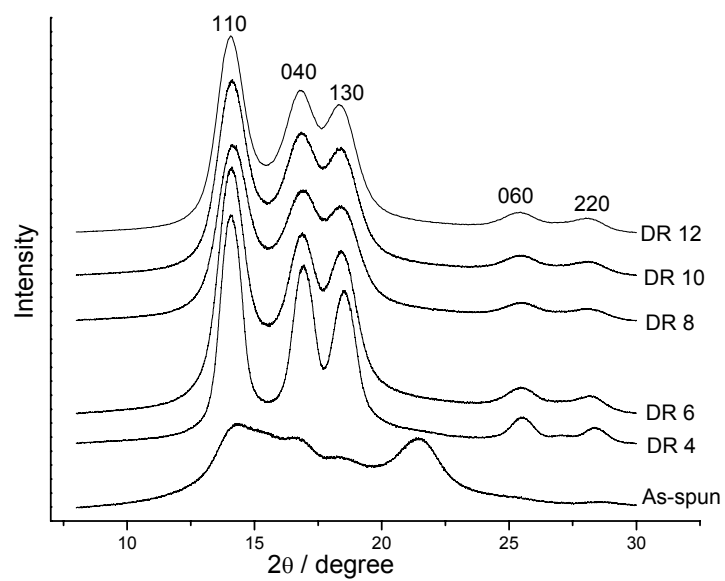


Figure 6. WAXD profiles of as-spun and neck drawn PP fiber.

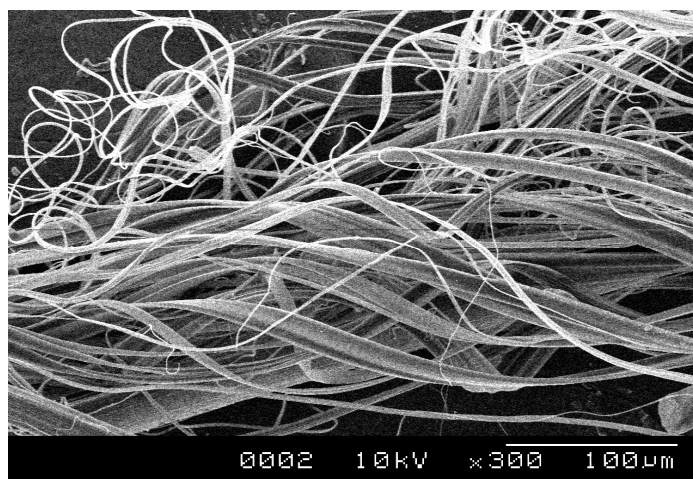


Figure 7. SEM image of fractured fibrillated PP (draw ratio 12) fiber.

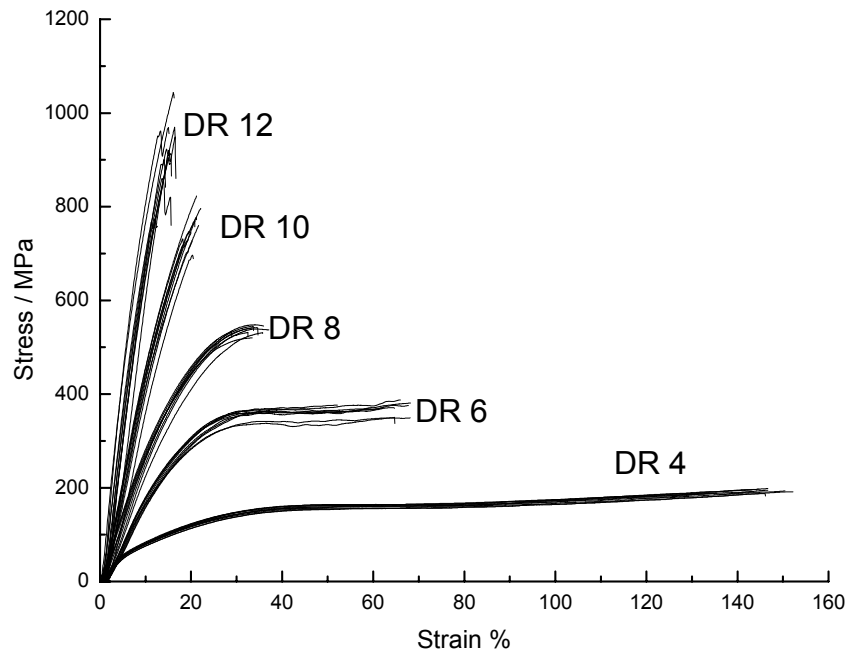


Figure 8. Stress-strain curves of the neck-drawn PP fibers.

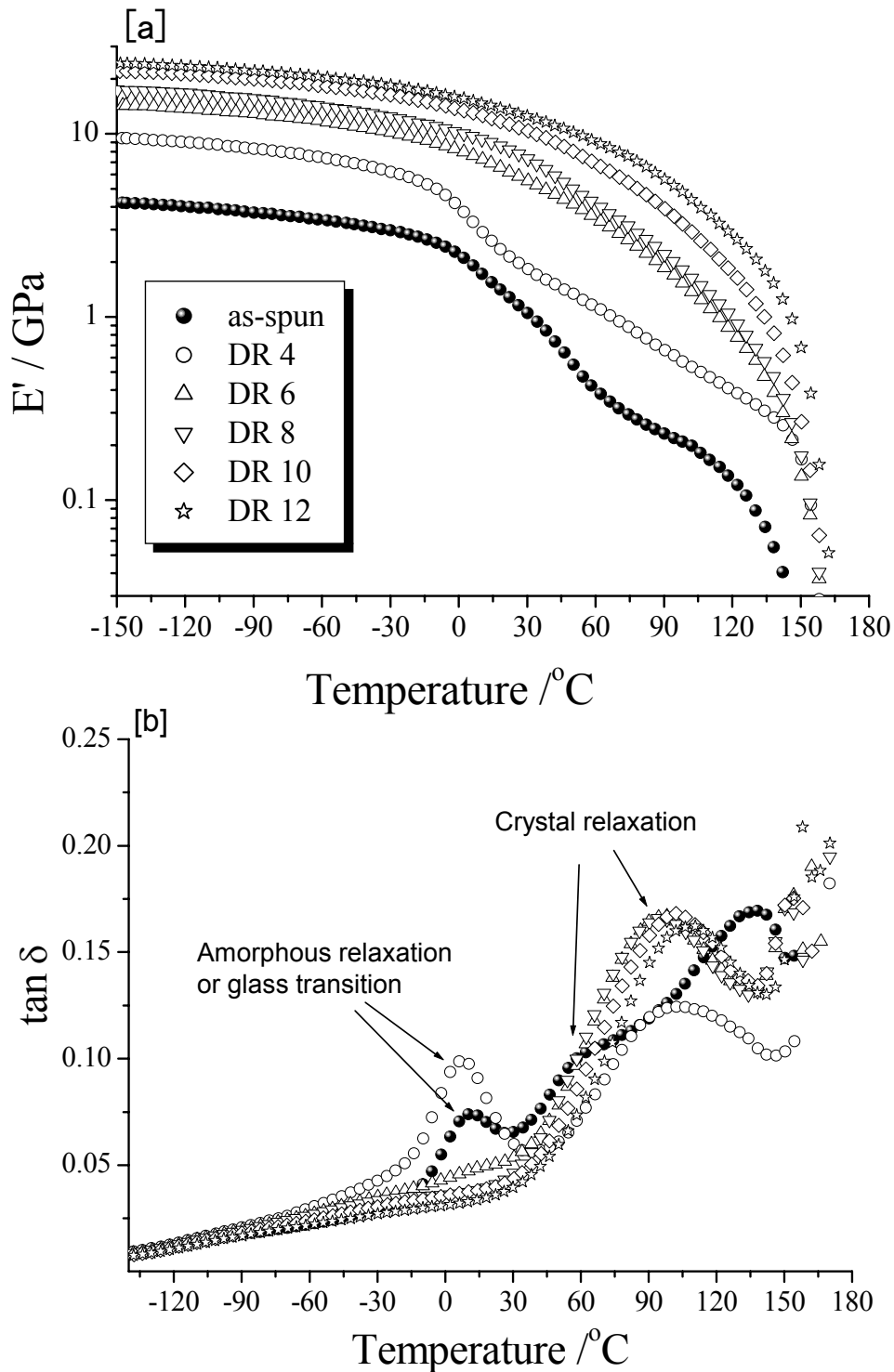


Fig. 9. (a) Storage modulus ( $E'$ ) and (b) loss tangent ( $\tan \delta$ ) curves of as-spun and neck drawn PP fibers.

Table 1: Characteristics of as-spun and flow drawn (draw ratio around 18) PP fibers.

Sample	Diameter $\mu\text{m}$	Birefringence $\times 1000$	Tensile Strength (MPa)	Young's Modulus (GPa)	Elongation at Break (%)
As-spun	149	6	80	0.8	671
Flow drawn	35	17	110	2.0	411

Table 2: Drawing Stress and Structure of neck-drawn PP fibers

Sample	Dia- meter $\mu\text{m}$	Drawing Stress MPa	Birefrin- gence $\times 1000$	Density $/\text{g cm}^{-3}$	Volume Crystallinity (%)	Crystal Orientation Factor ( $f_c$ ) (110)
As-spun	488	-	5	0.887	40.5	-
DR 4	254	8	25	0.889	43.3	0.880
DR 6	202	30	26	0.896	51.3	0.973
DR 8	186	52	28	0.898	54.3	0.974
DR 10	149	81	-	-	-	0.976
DR 12	139	126	-	-	-	0.979

Table 3: Tensile Properties of as-spun and neck-drawn PP fibers

Sample	Tensile Strength MPa	Young's Modulus GPa	Elongation at Break (%)
As-spun	50	0.5	1769
DR 4	190	2.6	144
DR 6	360	4.4	65
DR 8	530	5.8	33
DR 10	750	9.2	21
DR 12	910	11.0	15